Natural emodin reduces myocardial ischemia/reperfusion injury by modulating the RUNX1/miR-142-3p/DRD2 pathway and attenuating inflammation

XUEZHI ZHANG[1], QIAOJI QIN[2], XIANGHONG LV[3], YONGBIN WANG[2], FENG LUO[1] and LI XUE[4]

Departments of [1]Cardiology and [2]Emergency Internal Medicine, The Affiliated Hospital of Qingdao University, Qingdao, Shandong 266003; [3]Department of Pediatrics, The Qingdao Central Hospital, Qingdao, Shandong 266042; [4]Department of Endoscopy, The Affiliated Hospital of Qingdao University, Qingdao, Shandong 266003, P.R. China

Received March 16, 2022; Accepted August 18, 2022

DOI: 10.3892/etm.2022.11681

Abstract. Acute myocardial infarction is one of the leading causes of death worldwide. Although timely reperfusion could attenuate myocardial ischemia injury and reduce mortality, it causes severe secondary injury to the myocardium known as myocardial ischemia/reperfusion injury (MIRI) with unmet clinical needs. Emodin has a protective effect on MIRI in rodents. However, the precise mechanism underlying its pharmacological effect remains poorly understood. Accordingly, the present study used mRNA and microRNA (miRNA) sequencing based on MIRI mouse models to determine the mechanism involved. Emodin was found to prevent MIRI and attenuate the inflammation of myocardium in the MIRI model. In addition, by using an interdisciplinary approach, the present study uncovered that emodin suppressed the runt-related transcription factor 1 (RUNX1), which is a transcription factor of miR-142-3p, in either MIRI or the hypoxia/reoxygenation injury model. Furthermore, miR-142-3p can negatively regulate dopamine receptor D2 (DRD2), which acted as an anti-inflammatory factor to suppress NF-κB-dependent inflammation and prevent MIRI. These results were demonstrated by both cellular hypoxia/reoxygenation and mouse MIRI models. Overall, the present study provided an unrevealed molecular mechanism for emodin function. Emodin could inhibit NF-κB-triggered inflammation in MIRI by regulating the RUNX1/miR-142-3p/DRD2 pathway. Therefore, the RUNX1/miR-142-3p/DRD2 pathway presented a novel target for MIRI treatment, and the application of emodin in clinical practice may improve the treatment of MIRI.

Correspondence to: Professor Xuezhi Zhang, Department of Cardiology, The Affiliated Hospital of Qingdao University, 369 Shanghai Road, Qingdao, Shandong 266003, P.R. China
E-mail: zxz_1204@163.com

Abbreviations: AAR, area at risk; DRD2, dopamine receptor D2; H/R, hypoxia/reoxygenation; IL-6, interleukin-6; I/R, ischemia/reperfusion; MIRI, myocardial ischemia/reperfusion injury; RUNX1, runt-related transcription factor 1; TNF-α, tumor necrosis factor α

Key words: emodin, ischemia/reperfusion, inflammation, runt-related transcription factor 1, dopamine receptor D2

Introduction

Cardiovascular disease is one of the deadliest diseases worldwide and acute myocardial infarction has become one of the leading causes of death (1-4). Timely blood reperfusion to the ischemic heart tissue can limit the size of myocardial infarction and reduce mortality. Nevertheless, this treatment can further induce serious secondary injury to the myocardium known as myocardial ischemia/reperfusion injury (MIRI) (5-7). MIRI has complex pathological mechanisms, such as mitochondrial disorders, calcium overload and the production of reactive oxygen (8-10). Inflammation plays an important role in the pathophysiology of MIRI (11,12). MIRI activates the immunity-inflammation responses and increases the production of inflammasomes, leading to inflammatory cell infiltration and increased cytokine release in the heart (11,13,14). Likewise, hypoxia/reoxygenation (H/R), a model of MIRI, leads to the excessive release of inflammatory factors TNF-α and IL-6 from cardiac myoblast H9c2 cells and causes excessive death of H9c2 cells (15,16). Therefore, the pharmacological inhibition of cardiomyocyte inflammation can effectively protect the myocardium against MIRI.

Emodin, as an anthraquinone derivative extracted from traditional Chinese medicine rhubarb, possesses anti-inflammation, immune regulation and antioxidant properties (17,18). Emodin attenuates MIRI in rodents via various cellular functions and signaling pathways, but the precise mechanism underlying the attenuation of MIRI by emodin by modulating the inflammation response remains unknown (19,20).

A type of small non-coding RNA known as microRNA (miRNA/miR) negatively regulates gene expression during post-transcriptional processes by binding to the target mRNAs (21). MiRNAs are instrumental in the development of cardiac diseases, including MIRI (22). For instance, miR-384-5p alleviates MIRI in rats via the inhibition of the expression of Beclin-1 to suppress autophagy (23). miR-322

prevents MIRI by attenuating FBXW7-caused oxidative stress (24). However, whether emodin can attenuate inflammation in MIRI by regulating miRNAs and its upstream transcription factors remains unknown.

In the present study, it was further confirmed that emodin pretreatment could relieve ischemia/reperfusion (I/R) injury and inflammatory responses of mice myocardium. By using RNA sequencing combined with reverse transcription-quantitative PCR (RT-qPCR) and western blotting, emodin was shown to inhibit the expression of transcription factor RUNX1 and thus downregulated the transcriptional level of miR-142-3p in MIRI. The expression of RUNX1/miR-142-3p was confirmed both *in vivo* or *in vitro*. The present study's findings support an undiscovered model, whereby emodin inhibited RUNX1/miR-142-3p pathway and thus upregulated DRD2, which acts as an anti-inflammatory mediator that suppresses the NF-κB-dependent inflammation and prevents MIRI.

Materials and methods

Animals. A total of 80 male ICR mice (6-8-weeks old, weighing 25±3 g) were obtained from Beijing Vital River Laboratory Animal Technology Co., Ltd. and housed in a temperature-controlled animal room (23±1˚C), with relative humidity between 50-60% and daylight between 8:00-19:00. Food and water were freely accessible for the mice. Each group contained 5-6 mice in every independent experiment and a total of 80 mice were used in the project. All animal experiments were approved by the Animal Care and Use Committee of The Affiliated Hospital of Qingdao University (approval no. QYFYWZLL26907; approval date, March 20, 2021). Mice used in experiments were euthanized 24 h after establishing an MIRI model by intraperitoneal administration of an overdose of pentobarbital sodium (200 mg/kg), and the heart samples were harvested. After establishing the MIRI model, mouse health was monitored every other hour, including the ability to breathe normally, eat normally and move freely. Some of the mice were euthanized prior to the experimental endpoint if they went into dyspnea, lethargy, shock or decreased activity.

Experimental protocol for construction of MIRI model. ICR mice were randomly divided into three groups, namely: Sham group (control), MIRI group and emodin (MedChemExpress) treatment group (MIRI + emodin). Mice were intragastrically administrated with 10 mg/kg emodin or saline (vehicle) once a day for 7 consecutive days (day 1-7) before inducing the MIRI model. The MIRI model was performed 1 h after the last emodin treatment on day seven. To establish the MIRI model, the mice were anesthetized by intraperitoneal administration of 2% pentobarbital sodium (50 mg/kg) and were ventilated by using a rodent respirator. The thoracic cavity was opened, and the pericardium was cut open to expose the heart. The left anterior descending branch (LAD) of the coronary artery was ligated 2-mm away from its origin with surgical sutures for 60 min. A successful ligation was confirmed by the change of myocardial color from red to grayish white. The mice in the sham group were also anesthetized, and a suture was just passed under the LAD without obstruction. After a 60 min ligation of the LAD, myocardial blood flow was restored for 24 h to induce I/R injury before the heart was harvested for subsequent analysis.

Determination of area at risk (AAR) and infarct area. For the measurement of AAR and infarct area, 24 h after MIRI, the heart samples of the mice were perfused with Evans blue (1%) and subsequently incubated with 2.0% triphenyltetrazolium chloride (TTC) at 37˚C for 20 min. The non-ischemic myocardium was stained blue with Evans Blue. AAR was stained red by TTC, and the infarct area appeared pale after staining. The left ventricle (LV), AAR and infarct areas were determined using Image J 1.42q software (National Institutes of Health). The percentages of infarct area/AAR and AAR/LV were defined as the dead and ischemia level of myocardium, respectively.

Western blotting. The mice cardiac tissues (60-80 mg) or rat cardiac myoblast H9c2 cells were lysed in RIPA buffer (Thermo Fisher Scientific, Inc.). The supernatant was quantified with Pierce BCA protein assay reagent kit (Thermo Fisher Scientific, Inc.). Total protein (20 μg per sample) was loaded and separated in 10% or 12% SDS-PAGE, and transferred to a PVDF membrane (MilliporeSigma). After blocking in TBST (0.1% Tween-20) containing 5% fat-free milk at room temperature for 1 h, the membrane was incubated with primary anti-RUNX1 (1:1,000; cat. no. ab229482; Abcam), anti-DRD2 (1:500; cat. no. bs-20730R; BIOSS), anti-phosphorylated (p-)P65 subunit of NF-κB (1:1,000; cat. no. ab76302; Abcam), anti-NF-κB P65 subunit (1:1,000; cat. no. bs-20355R; BIOSS), anti-TNF-α (1:500; cat. no. bs-2081R; BIOSS), anti-IL-6 (1:500; cat. no. ab259341; Abcam) or anti-β-tubulin (1:1,000; cat. no. ab18207; Abcam) antibodies respectively, overnight at 4˚C. After washing three times in TBST, the membranes were incubated with HRP-conjugated goat anti-rabbit secondary antibody (1:10,000; cat. no. ab191866; Abcam) for 1.5 h at room temperature. Protein band signals were detected using ECL program (Thermo Fisher Scientific, Inc.) under chemiluminescence detector (Bio-Rad Laboratories). The expression of target protein was normalized to β-tubulin using Image Lab Software (Bio-Rad Laboratories).

Hematoxylin-eosin (H&E) and Masson staining. Paraformaldehyde (4%) was used to immobilize myocardial tissue samples at 4˚C for 24 h. Subsequently, samples were dehydrated with gradient ethanol (70-100%) for 30 min before treating with 50 and 100% xylene, respectively, at room temperature for 1.5 h for transparency. After embedding in paraffin, the processed tissues were cut into 5-μm thick slices. After deparaffinization in an incubator (60˚C; 2 h), followed by incubation twice with 100% xylene for 20 min and rehydration in descending alcohol (100-70%) at room temperature, the slices were stained with Masson's Trichrome Stain kit (Beijing Solarbio Science & Technology Co., Ltd.) or H&E (Beijing Solarbio Science & Technology Co., Ltd.) according to the products' instructions. The results were observed under a light microscope (Eclipse TS100; Nikon Corporation) and images were captured.

Immunohistochemistry. The 5-μm thick paraffin slices of myocardium were deparaffinized in an incubator (60˚C; 2 h) and rehydrated in a descending alcohol series before washing

with distilled water. After antigen recovery, 3% H_2O_2 was used to eliminate the activity of endogenous peroxidase. The processed slices were blocked with 5% BSA for 30 min at room temperature before incubation with anti-TNF-α (1:200; cat. no. ab205587; Abcam) in a sealed wet box at 4˚C overnight, and then incubated with HRP-conjugated anti-rabbit secondary antibody (1:2,000; ab191866; Abcam) at room temperature for 1 h. After incubation with diaminobenzidine reagents (cat. no. DA1016; Beijing Solarbio Science & Technology Co., Ltd.) for color detection, the slices were counterstained with hematoxylin at room temperature for 3 min and images were captured under a light microscope (Eclipse TS100; Nikon Corporation).

Creatine kinase (CK), CK-MB and lactate dehydrogenase (LDH) assay. The expression levels of creatine kinase, CK-MB and lactate dehydrogenase in the serum of the mice were measured using Creatine Kinase Assay kit (cat. no. BC1145, Beijing Solarbio Science & Technology Co., Ltd.), CK-MB Elisa kit (cat. no. SEKM-0152; Beijing Solarbio Science & Technology Co., Ltd.) and LDH Activity Detection kit (cat. no. BC0685, Beijing Solarbio Science & Technology Co., Ltd.), respectively.

Cell culture and establishment of H/R model. Rat cardiac myoblast H9c2 cells were obtained from the Cell Bank of the Chinese Academy of Sciences and cultured with Dulbecco's modified Eagle medium (Gibco; Thermo Fisher Scientific, Inc.) with 10% fetal bovine serum (Gibco; Thermo Fisher Scientific, Inc.) and 100 U/ml streptomycin and penicillin (Gibco; Thermo Fisher Scientific, Inc.) in normal gas mixture (95% air and 5% CO_2) at 37˚C. The H9c2 cells were incubated in gas mixture containing 94% N_2, 5% CO_2 and 1% O_2 for 3 h to induce hypoxia injury before removing to a normoxic incubator for another 3 h to maintain reoxygenation (19,25).

Cell transfection. Lipofectamine® 3000 (Invitrogen) was used in transfection. Negative control (NC) mimic (cat. no. miR1N0000001-1-5) and miR-142-3p mimic (cat. no. miR10000155-1-5) were obtained from Guangzhou RiboBio Co., Ltd. NC mimic or miR mimic at a final concentration of 50 nM were transfected to a H9c2 cell-seeded 6-well plate at 37˚C for 4 h. The complementary DNAs (cDNAs) of RUNX1 and DRD2 were subcloned to pcDNA3.1 vector (Invitrogen: Thermo Fisher Scientific, Inc.), and 2 μg/well of these cDNAs were transfected into a H9c2 cell-seeded 6-well plate at 37˚C for 4 h. The control (without H/R injury) and H/R groups were transfected with pcDNA3.1 vector as the negative control. Subsequent experiments were performed 48 h after transfection.

Inhibition of miR-142-3p and overexpression of DRD2 in vivo. The mmu-miR-142-3p antagomir (miR-142-3p anti-ago; cat. no. miR-311620131514-4-5) and negative control antagomir (NC anti-ago; cat. no. miR3N0000001-4-5) were purchased from Guangzhou RiboBio Co., Ltd., and administered by tail vein injection with 5 nmol three times (once every two days). The MIRI models were established after 20 days from the first injection. To determine the effect of DRD2 in MIRI, recombinant adeno-associated virus (AAV) expressing DRD2 (AAV-DRD2) was purchased from Hanbio Biotechnology Co., Ltd. and administered once via a 50-μl tail vein injection, while the control and MIRI groups were injected with AAV control (AAV-Ctrl; Hanbio Biotechnology Co., Ltd.). The MIRI models were established 20 days after the injection.

RT-qPCR analysis. Total RNAs were extracted from myocardium or H9c2 cells using TRIzol® reagent (Invitrogen; Thermo Fisher Scientific, Inc.). A total of 1 μg of extracted total RNA was reverse-transcribed to cDNAs by using a Reverse Transcription kit (Takara Bio, Inc.) according to the manufacturer's instructions. Primers were obtained from Sangon Biotech Co., Ltd. RT-qPCR was performed using SYBR® Green Master Mix (Takara Bio. Inc.) in a 20 μl reaction system containing specific primers, and primer sequences are listed in Table SI. The mRNA levels of target genes were detected using the CFX96 real time PCR detection system (Bio-Rad Laboratories). For miR-142-3p (sequence: 5'-UGUAGUGUU UCCUACUUUAUGGA-3') analysis, the stem-loop reverse transcription primer sequence was 5'-GTCGTATCCAGTGCA GGGTCCGAGGTATTCGCACTGGATACGACTCCATA-3', and the qPCR forward primer was 5'-TGTAGTGTTTCCTAC TT-3' and the reverse primer was 5'-GTGCAGGGTCCGAGG T-3'. The thermocycling conditions used for RT-qPCR were as follows: Cycle at 94˚C for 5 min, followed by 40 cycles (10 sec at 94˚C for denaturation, 15 sec at 60˚C for annealing and 20 sec at 72˚C for extension) and a final elongation at 72˚C for 5 min. The relative expression levels of miRNA and genes were normalized to that of internal control U6 and GAPDH, respectively, and analyzed by using $2^{-\Delta\Delta Cq}$ method (26).

RNA purification. Total RNAs were extracted from the mice hearts of MIRI and MIRI + emodin groups by using TRIzol® reagent (cat. no. 15596026; Invitrogen; Thermo Fisher Scientific, Inc.) at 24 h after performing MIRI. RNA samples were stored in dry ice and submitted to Shanghai Personal Biotechnology Co., Ltd. for high-throughput sequencing. Quality control for the RNA samples was carried out by using an Agilent 2100 Bioanalyzer with Agilent RNA 6000 Nano Kit (Agilent Technologies, Inc.). RNA samples with the standard of total RNAs >8 μg, concentration >250 ng/μl, the ratio of 28S/18S >1.5 and the RNA integrity number >8 were selected for establishment of mRNA and miRNA libraries.

Library preparation and RNA sequencing. The mRNAs were separated from the total RNAs using the olig-dT method, and cut into 200 bp fragments by Mg^{2+} randomly. Fragments were reverse transcribed to cDNAs, which were purified and end modified before being connected to adapters. The cDNA fragments of 200-300 bp were chosen for PCR amplification and library construction. RNAs (18-30 nt) were separated from total RNAs, and selected for construction for microRNA sequencing library. The final library was amplified with phi29 DNA polymerases (Thermo Fisher Scientific, Inc.) to make a DNA nanoball (DNB) which had >300 copies of one molecule. DNBs were loaded into the patterned nanoarray and single end 150 base reads were generated on the DNBSEQ-T7 sequencing platform (MGI; BGI Group). Quality control of raw reads was performed using the SOAPnuke software

(BGI Group). The following reads were filtered: i) The reads containing the adaptor, ii) the reads whose N content was >5%, and iii) low-quality reads (reads with bases having a quality score <10 as the proportion of total bases in the reads that were >20% as low-quality reads). The filtered clean reads obtained from each sample were packed in the form of FASTQ, with an average size of 6.62 Gb. Hierarchical Indexing for Spliced Alignment of Transcripts (HISTAT) was used to map RNA-sequencing reads to the reference genome. Firstly, the HISTAT global FM index was used to anchor the position of partial sequences in each read on the genome, and then the partial genome indexes of these alignment positions was used to align the remaining sequences of each read to extend the alignment area. Differentially expressed genes were analyzed with Bioconductor DESeq2 version 1.12.3 (https://www.rdocumentation.org/packages/DESeq2). The criteria for determining differentially expressed miRNAs and transcription factors are the $\log_2$ fold-change ($\log_2$FC) >2 or <-2 with a q value <0.05 and the $\log_2$FC >1 or <-1 with q value <0.05, respectively.

Prediction of potential transcription factors (TFs) and target genes of miRNAs. Based on the differentially expressed miRNAs, the upstream TFs were predicted using TransmiR v2.0 database (http://www.cuilab.cn/transmir), an easy-accessible public tool, which integrates experimentally verified TF-miRNA regulatory relationships from the publications (27). In addition, the downstream target genes of miRNAs were also predicted using miRWalk database (http://mirwalk.umm.uni-heidelberg.de/), which is freely available and presents validated and predicted information on miRNA-target interaction (28).

ELISA. The cytokines released from the myocardium were measured by using TNF-α (cat. no. ab208348; Abcam) and IL-6 (cat. no. ab222503; Abcam) ELISA kits. Assays were performed according to the manufacturer's instructions. The absorbance at 450 nm was measured using a Sunrise microplate reader (Tecan Group, Ltd.).

Statistical analysis. The data were collected from at least three independent experiments and statistical analysis was performed using one-way analysis of variance (ANOVA) followed by Tukey's multiple comparisons test in GraphPad Prism 7.0 (GraphPad Software, Inc.). All data were expressed as the mean ± standard deviation. P<0.05 was considered to indicate a statistically significant difference.

Results

Emodin protects against MIRI in mice. To investigate the underlying molecular mechanism for natural emodin attenuation of MIRI, emodin was intragastrically administrated to the mice for 7 consecutive days before inducing the MIRI model. As shown in Fig. 1A, Evans Blue/TTC staining showed that I/R resulted in myocardial infarction. By contrast, pretreatment with emodin markedly attenuated the size of myocardial infarction induced by I/R, and the productions of LDH, CK and CK-MB were subsequently significantly suppressed compared with the MIRI group (Fig. 1B). Moreover, the alleviative effect was confirmed using histopathological staining. H&E staining images displayed that the cardiomyocytes in the MIRI group were disordered and swollen, and the sarcolemma was disrupted compared with the control (sham) group (Fig. 1C). Pretreatment with emodin markedly reversed these pathological changes. The Masson staining results showed that the myocardial collagen fiber deposition (stained blue) in the MIRI group increased, and emodin pretreatment markedly reduced the collagen deposition (Fig. 1C).

Next, the regulative action of emodin on the process of inflammatory responses after MIRI was tested. Immunohistochemical staining displayed an upregulated expression of TNF-α in the myocardial sections after I/R injury compared with the control group (Fig. 1D), and emodin pretreatment suppressed the expression of TNF-α. The TNF-α and IL-6 secretions from myocardium evoked by I/R injury were also significantly reduced in the emodin pretreatment group (Fig. 1E). Therefore, the inhibition of inflammation response by emodin prevented MIRI.

Emodin suppresses the RUNX1/miR-142-3p pathway in either MIRI or hypoxia/reoxygenation injury. To determine the molecular mechanism underlying inhibition of inflammation during MIRI by emodin, myocardium from MIRI and MIRI + emodin groups were collected and RNA transcripts and microRNA sequencing were performed using the DNBSEQ-T7 sequencing platform. The sequencing data were normalized to the MIRI group. As shown in Table SII, 34 differentially expressed miRNAs were screened out. To determine the key transcription factors (TFs) that regulated the expression of these differentially expressed miRNAs, the TransmiR v2.0 database was used to match the regulatory networks between the differentially expressed TFs and miRNAs. A total of four pairs of differentially expressed regulatory networks between TFs and miRNAs were matched (Table SIII), among which only two pairs displayed consistent trends of downregulation. For an unprejudiced analysis, the RUNX1/miR-142-3p pathway with the most obvious change was uncovered as the candidate for the modulation of MIRI-induced inflammation by emodin (Table SIII).

The present study examined whether the level of miR-142-3p could be regulated by the transcription factor RUNX1 in the pathological process of MIRI. The mRNA expression levels of transcription factor RUNX1 were significantly increased after H/R injury in H9c2 cells or MIRI (Fig. 2A and B). RUNX1 protein levels were also detected using western blotting and showed a consistent trend with the mRNA level (Fig. 2C-F). As expected, the expression of miR-142-3p was also significantly increased after H/R injury in H9c2 cells or MIRI (Fig. 3A and B). These results further identified that RUNX1 acted as a transcription factor, and that it also promoted the expression of miR-142-3p in cardiomyocytes.

Next, the inhibitory effect of emodin on the RUNX1/miR-142-3p pathway was verified. Pretreatment with emodin attenuated the expression levels of either RUNX1 or miR-142-3p in both the myocardium with I/R injury and in H9c2 cells with H/R compared with the model groups (Figs. 2 and 3). These results supported that the RUNX1/miR-142-3p pathway was downregulated in emodin-pretreated groups based on bioinformatical analysis (Table SIII). Therefore, the overactive

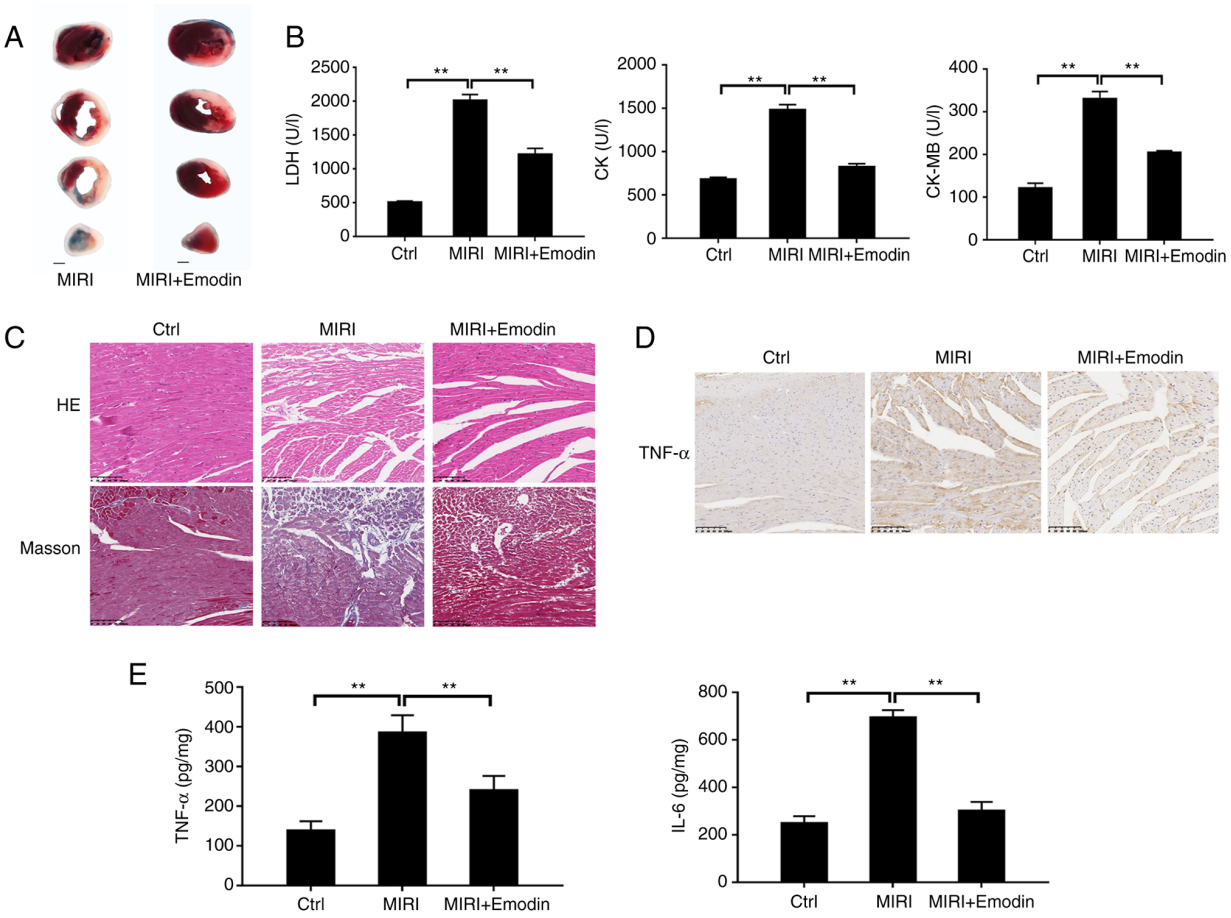

Figure 1. Emodin relieves MIRI in mice. (A) Representative Evans Blue/triphenyltetrazolium chloride staining images of myocardial sections from the indicated groups (scale bar, 1 mm). (B) Summary for the mean release levels of LDH, CK and CK-MB from the serums of mice after MIRI with or without emodin pretreatment. (C) Representative H&E (upper panels) and Masson (lower panels) staining images of myocardial sections after MIRI with or without emodin pretreatment (scale bar, 100 μm). (D) Immunohistochemical staining for detecting the expression level of TNF-α in myocardial sections (scale bar, 100 μm). (E) Summary of the secretion of TNF-α and IL-6 from the heart tissues evoked by MIRI or treatment with emodin. n=5 mice for each group. **P<0.01. MIRI, myocardial ischemia/reperfusion injury; H&E/HE, hematoxylin and eosin; LDH, lactate dehydrogenase; CK, creatine kinase; Ctrl, control.

RUNX1/miR-142-3p pathway was involved in the inflammatory process of MIRI, and emodin could suppress the RUNX1/miR-142-3p pathway.

MiR-142-3p negatively regulates the expression of DRD2. With few exceptions, miRNAs theoretically negatively regulate the expression of their targeted mRNAs (29). To identify the downstream mRNAs targeted by miR-142-3p, two subsets of genes were defined, among which subset one represents predicted targets for miR-142-3p by using the miRWalk database and subset two represents upregulated differentially expressed genes ($\log_2$FC >2 with q value <0.05) in the emodin-treated group based on transcriptome sequencing. The 12 overlapped genes between subset one and two are defined as the potential targets for miR-142-3p (Table SIV).

To further validate the key gene targeted by miR-142-3p, the present study used RT-qPCR to detect the expression of these 12 potential genes in H9c2 cells overexpressing miR-142-3p mimic. As shown in Fig. S1, transfection with miR-142-3p mimic in H9c2 cells for 48 h caused a significant increase in the expression of miR-142-3p compared with the negative control mimic group. The mRNA levels of KCNA2, TNIP3 and DRD2 in the miR-142-3p mimic-overexpressed group were significantly downregulated compared with the NC mimic group, among which DRD2 showed the most obvious downregulation (Fig. 4A). Accordingly, DRD2 was chosen as a candidate. To further confirm this, a miR-142-3p antagomir (miR anti-ago) was used to reduce miR-142-3p levels in mice myocardium (Fig. S1B), and the protein expression was detected using western blotting. As expected, the protein level of DRD2 was significantly increased in the miR-142-3p antagomir (anti-ago) pretreated myocardium after I/R injury compared with the MIRI group (Fig. 4B and C). Besides, the protein level of DRD2 also significantly increased in the emodin-treated H9c2 cells with H/R injury compared with the untreated group (Fig. 4D and E). These data further confirmed that emodin treatment attenuated the level of miR-142-3p, which negatively regulated the expression of DRD2. The protein level of DRD2 was significantly increased in the emodin-pretreated myocardium after I/R injury compared with the MIRI group (Fig. 4F and G). Therefore, emodin upregulated DRD2 after MIRI by downregulating miR-142-3p.

RUNX1/miR-142-3p/DRD2 pathway can regulate the NF-κB-mediated inflammatory response in H9c2 cells with H/R injury. Next, RUNX1, miR-142-3p mimic and DRD2

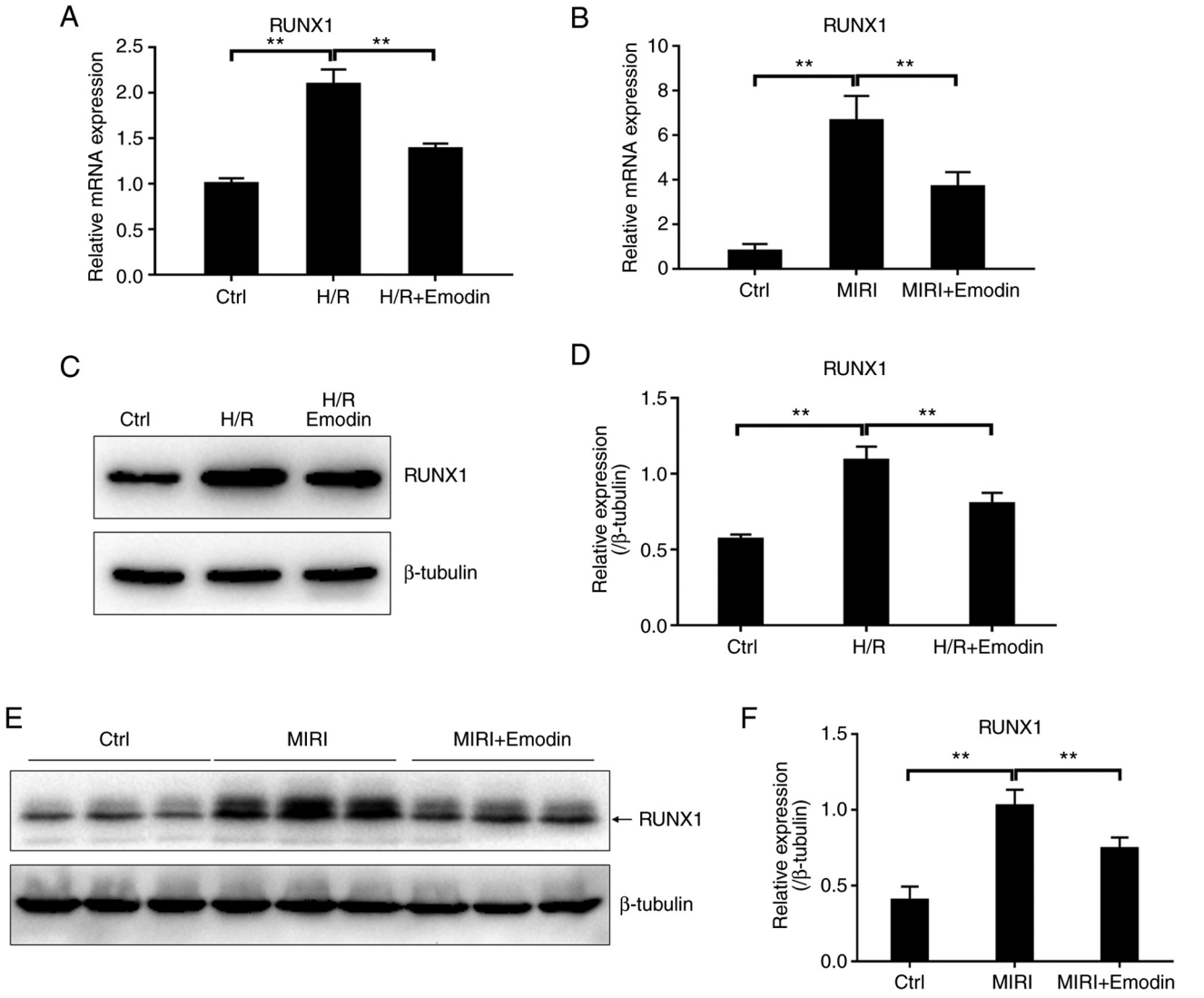

Figure 2. Emodin attenuates the expression level of transcription factor RUNX1 induced by either H/R injury or MIRI. (A) RUNX1 gene expression in H9c2 cells with H/R injury or emodin treatment was determined using RT-qPCR. n=5. (B) The mRNA level of RUNX1 in myocardium with MIRI or emodin treatment was measured using RT-qPCR. n=5. (C) RUNX1 protein was detected by western blotting in H9c2 cells with H/R injury or emodin treatment. (D) Summary for the protein expression level of RUNX1 based on (C). n=3. (E) RUNX1 protein expression in myocardium with MIRI or emodin treatment was detected by western blotting. Three bands represent three independent samples. (F) Summary for the protein expression level of RUNX1 based on (E). n=3. **P<0.01. RUNX1, runt-related transcription factor 1; H/R, hypoxia/reoxygenation; MIRI, myocardial ischemia/reperfusion injury; RT-qPCR, reverse transcription-quantitative PCR; Ctrl, control.

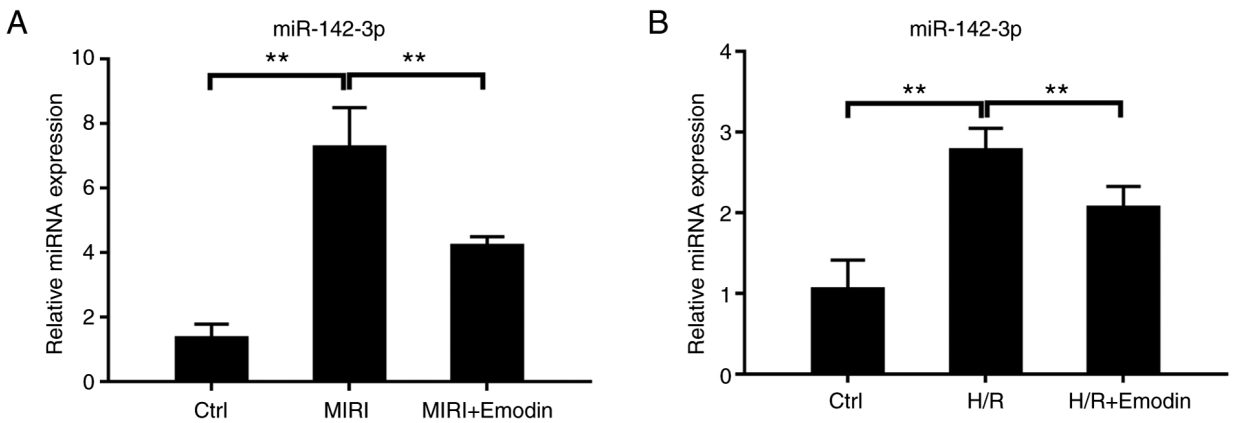

Figure 3. Emodin treatment suppresses MIRI, and H/R injury induced the expression of miR-142-3p. (A) The level of miR-142-3p in myocardium with MIRI or emodin treatment was determined using RT-qPCR. n=5. (B) RT-qPCR for determination of the expression level of miR-142-3p in H9c2 cells under H/R injury or emodin treatment conditions. **P<0.01. miRNA, microRNA; MIRI, myocardial ischemia/reperfusion injury; H/R, hypoxia/reoxygenation; RT-qPCR, reverse transcription-quantitative PCR; Ctrl, control.

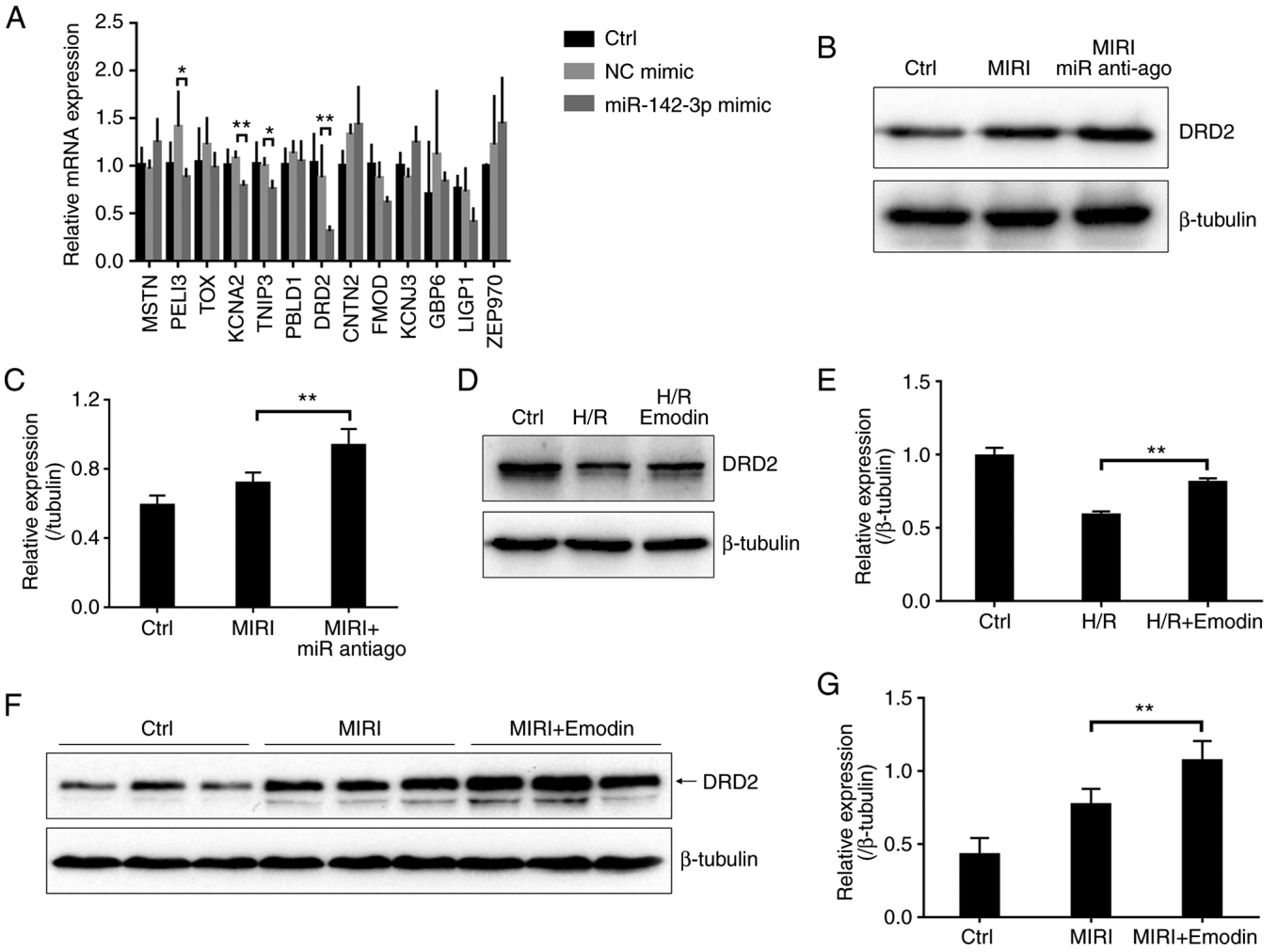

Figure 4. miR-142-3p negatively regulates the expression of DRD2. (A) Reverse transcription-quantitative PCR for the identification of the downstream target gene of miR-142-3p by overexpressing miR-142-3p mimic in H9c2 cells. n=4. (B) The DRD2 protein levels were detected by western blotting in cardiac tissues with MIRI or miR-142-3p antagomir (anti-ago) treatment. (C) Summary for the protein expression of DRD2 based on (B), n=3. (D) DRD2 protein levels were detected by western blotting in H9c2 cells with H/R injury or emodin treatment. (E) Summary for the protein expression of DRD2 based on (D), n=3. (F) DRD2 protein levels were measured using western blotting in cardiac tissues with MIRI or emodin treatment. Three bands represent three independent samples. (G) Summary for the protein expression of DRD2 based on (F), n=3. *P<0.05, **P<0.01. NC, negative control; MIRI, myocardial ischemia/reperfusion injury; anti-ago, antagomir; DRD2, dopamine receptor D2; Ctrl, control; miR, microRNA; H/R, hypoxia/reoxygenation.

were overexpressed in H9c2 cells and their roles were evaluated in the modulation of inflammation (Fig. S2). As shown in Fig. 5A and B, the production of cytokine TNF-α in the RUNX1 overexpression group and IL-6 in the RUNX1 and miR-142-3p mimic overexpression groups from H9c2 cells after H/R injury were significantly increased compared with the H/R injury group. In addition, the p-P65 subunit of NF-κB was upregulated in these two groups compared with the H/R injury group (Fig. 5C). Conversely, the DRD2 overexpression group showed a significantly reduced production of TNF-α and IL-6 compared with the H/R group (Fig. 5A and B), and the p-P65 subunit of NF-κB was also downregulated (Fig. 5C). Therefore, RUNX1 and miR-142-3p acted as pro-inflammatory factors, and DRD2 acted as an anti-inflammatory factor to regulate the NF-κB-mediated inflammatory responses.

Either the inhibition of miR-142-3p or overexpression of DRD2 attenuates NF-κB-mediated inflammatory response in MIRI model of mice. Next, miR-142-3p anti-ago or adeno-associated virus (AAV) carrying DRD2 (AAV-DRD2) were used to further validate the roles of miR-142-3p and DRD2 in modulating the inflammation *in vivo* after MIRI. As shown in Fig. S3, tail vein injection with AAV-DRD2 caused a significant increase of DRD2 in mice cardiac tissues 20 days after the first injection compared with the AAV control (AAV-Ctrl) injection group. The secretions of TNF-α and IL-6 from the myocardium were significantly inhibited in the anti-ago-pretreated and AAV-DRD2-overexpressed groups after MIRI compared with the MIRI group (Fig. 6A and B). AAV-DRD2-overexpression also resulted in a significant decrease in p-P65 protein, and the anti-ago treatment showed a downregulated trend (Fig. 6C and D). Therefore, the inhibition of miR-142-3p or activation of DRD2 suppresses the NF-κB-mediated inflammatory process. Taken all together, the present study presented a novel model, in which the inhibition of the expression of RUNX1 and miR-142-3p by emodin lead to the upregulation of DRD2 which acted as an anti-inflammatory factor to suppress NF-κB-dependent inflammation and prevent MIRI (Fig. 6E).

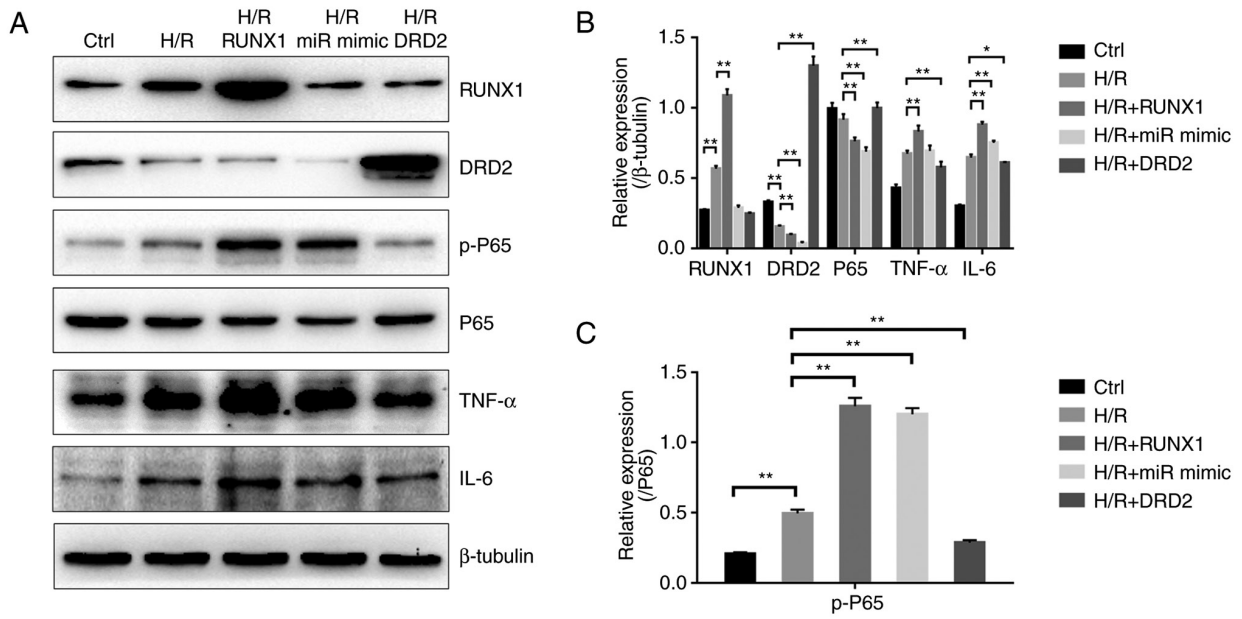

Figure 5. RUNX1/miR-142-3p/DRD2 pathway regulates the NF-κB-dependent inflammatory responses in H9c2 cells with H/R injury. (A) The NF-κB dependent inflammatory response was regulated by overexpression of RUNX1, miR-142-3p mimic and DRD2 in H9c2 cells with H/R injury and detected using western blotting. (B) Bar diagram showing the protein expression levels of RUNX1, DRD2, P65, TNF-α and IL-6 based on (A). n=3. (C) Bar diagram showing the protein expression of functional p-P65 subunit of NF-κB based on (A). n=3. *P<0.05, **P<0.01. H/R, hypoxia/reoxygenation; DRD2, dopamine receptor D2; p-, phosphorylated-; miR, microRNA; Ctrl, control.

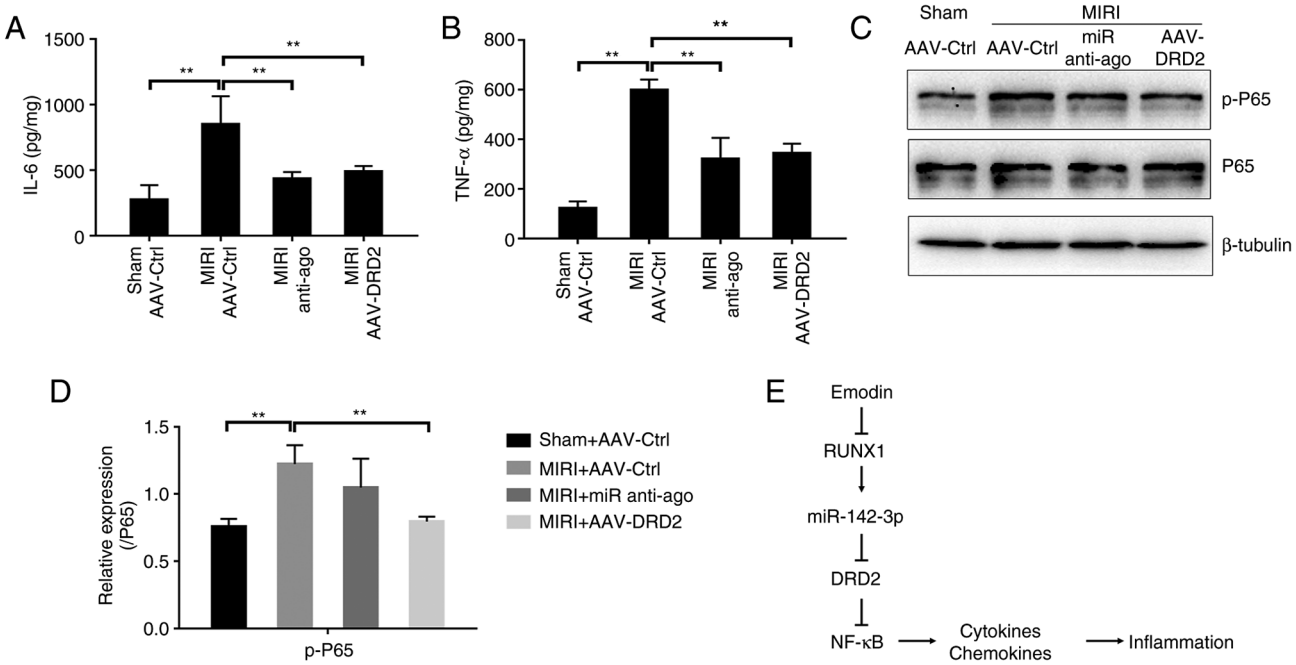

Figure 6. Inhibition of miR-142-3p or overexpression of DRD2 suppresses NF-κB-mediated inflammation in MIRI model of mice. The secretions of inflammatory cytokines (A) IL-6 and (B) TNF-α in cardiac tissues with MIRI of mice were measured by ELISA under the conditions of pretreatment with miR-142-3p antagomir (anti-ago) or overexpression of AAV-DRD2. n=4. (C) P65 and p-P65 were detected using western blotting to determine the activity of NF-κB. (D) Bar diagram showing the protein expression of p-P65 based on (C). n=3. (E) The schematic model for the anti-inflammation action of emodin in MIRI model of mice. **P<0.01. DRD2, dopamine receptor D2; MIRI, myocardial ischemia/reperfusion injury; anti-ago, antagomir; AAV, adeno-associated virus; p-, phosphorylated-; Ctrl, control; miR, microRNA.

Discussion

The present study aimed to investigate the link between emodin treatment and inflammation responses during MIRI. Results showed that emodin suppressed the expression of RUNX1/miR-142-3p in cardiomyocytes and contributed to an increased level of DRD2. Then, DRD2 inhibited the phosphorylation of NF-κB, thus reducing the production of inflammatory cytokines TNF-α and IL-6 (Fig. 6E). These findings not only described a novel molecular basis underlying

the action of emodin attenuation of MIRI, but also suggested that the pharmacological inhibition of RUNX1/miR-142-3p or activation of DRD2 may lead to a therapeutic potential for MIRI.

A number of cytokines and chemokines are released from the myocardium after I/R injury, leading to either apoptosis or cell death (30,31). NF-κB regulates the transcription of various pro-inflammatory genes implicated in disease processes (32). Emodin exerts anti-inflammatory action by inhibiting the transcription factor NF-κB (33,34). For example, emodin displays its anti-arthritic action by inhibiting the NF-κB pathway and pro-inflammatory factors in an arthritic model of mice induced by collagen (35,36). Besides, emodin can relieve corneal injury and improve the corneal structure by inhibiting the activation of NF-κB and c-JunN-terminal kinase (37,38). Although emodin inhibits the NF-κB-dependent inflammation in MIRI, the link between emodin and NF-κB is poorly reported (39). By using an unprejudiced analysis through RNA sequencing combination with qPCR and western blotting, the present study identified the downregulated transcription factor RUNX1 as the downstream target regulated by emodin. The present study further verified that RUNX1 controlled the expression of miR-142-3p and may serve as the initial effector to modulate emodin-mediated anti-inflammatory action in cardiomyocytes. RUNX1-overexpression can directly enhance the inflammatory responses in H9c2 cells. This finding is consistent with the observation that the downregulation of RUNX1 prevents cardiac remodeling (40,41). Therefore RUNX1, as a proinflammatory factor, participates in MIRI and the inhibition of RUNX1 may present a novel therapeutic strategy for MIRI. In the present study, the RUNX1-triggered miR-142-3p/DRD2 pathway was further confirmed in MIRI models and H9c2 cells with the H/R model. These findings complement the gap of signaling pathways between emodin and NF-κB, and suggest that the RUNX1/miR-142-3p/DRD2 pathway acts as a novel therapeutic target for MIRI and emodin may provide a therapeutic potential for MIRI.

The toxicity of emodin has been previously assessed (42). According to the United States National Toxicology Program (CAS no. 518-82-1), emodin at daily oral doses of 15, 35 or 70 mg/kg for 12 months does not affect the survival, body weight and food consumption of mice (43). Emodin at an oral dose of 100 mg/day has been investigated in a clinical trial (trial no. NCT00801268) for autosomal dominant polycystic kidney disease in the USA. A type of Chinese herb tablet, Sanhuangpian (Chinese FDA approval no. Zhunzi Z37021116) containing main active ingredient, emodin 12 mg, has been approved in China for inflammatory diseases. Therefore, the application of emodin in clinical practice may improve the treatment of MIRI.

MiRNAs, as small non-coding RNAs, modulate the transcription level of various genes that are implicated in the determination of apoptosis, necrosis, inflammation and fibrosis (44-46). The role of miRNAs in MIRI has been extensively studied throughout the last decade. Early changes (increase or decrease) of miRNAs occur in the myocardium in response to MIRI (47-49). The pharmacological or genetic regulation of these miRNAs can govern the pathological process of MIRI; therefore, miRNAs are regarded as therapeutic targets for heart diseases (47,50-52). In the present study, the miR-142-3p level decreased in response to emodin and further confirmed it as a pro-inflammatory factor in MIRI. Therefore, the specific inhibition of miR-142-3p could provide an alternative therapeutic strategy for MIRI. The mRNA of DRD2 as a target of miR-142-3p was also verified in the present study.

DRD2 is an anti-inflammatory critical component that controls innate immunity in the central nervous system (53). This is consistent with the present study's findings that either inhibition of miR-142-3p by specific antagomir or reduction of the transcription of miR-142-3p by the emodin/RUNX1 pathway could increase DRD2 expression levels in mice myocardium. In addition, DRD2-overexpression in H9c2 cells or myocardium of mice significantly reduced the levels of TNF-α, IL-6 and phosphorylated NF-κB. Although it cannot be excluded that emodin and miR-142-3p may directly regulate the NF-κB cytoplasmic binding or activity, these results at least partially show that upregulation of DRD2 by the emodin/RUNX1/miR-142-3p axis could suppress the NF-κB-mediated inflammatory responses.

In summary, the present study not only presented a novel molecular basis for protection against MIRI by emodin, but also suggested that the pharmacological modulation of the RUNX1/miR-142-3p/DRD2 pathway to suppress inflammatory responses of cardiomyocytes may be beneficial for the treatment of MIRI or other related heart diseases. Moreover, emodin may provide a potential therapeutic approach for MIRI.

Acknowledgements

Not applicable.

Funding

This project was financially supported by grants from the Qingdao 2020 Scientific Research Plan of Traditional Chinese Medicine (grant no. 2020-zyy058) and Youth Scientific Research Fund Project of the Affiliated Hospital of Qingdao University (grant no. 3095).

Availability of data and materials

The raw RNA sequencing data reported in this paper have been deposited in the Genome Sequence Archive (GSA) in National Genomics Data Center, China National Center for Bioinformation, Chinese Academy of Sciences (GSA accession number: CRA007195), and that are publicly accessible at https://ngdc.cncb.ac.cn/gsa/browse/CRA007195. The datasets used and/or analyzed during the current study are available from the corresponding author on reasonable request.

Authors' contributions

XZ, XL and LX designed this project. XZ, QQ, XL, YW and FL performed experiments and analyzed data. XZ and QQ wrote the manuscript. All authors have read and approved the final manuscript. XZ and QQ confirm the authenticity of all the raw data.

Ethics approval and consent to participate

All animal experiments were approved by the Animal Care and Use Committee of The Affiliated Hospital of Qingdao University (approval no. QYFYWZLL26907).

Patient consent for publication

Not applicable.

Competing interests

The authors declare that they have no competing interests.

References

1. Edmondson D and von Känel R: Post-traumatic stress disorder and cardiovascular disease. Lancet Psychiatry 4: 320-329, 2017.
2. Andersson C and Vasan RS: Epidemiology of cardiovascular disease in young individuals. Nat Rev Cardiol 15: 230-240, 2018.
3. Rout A, Tantry US, Novakovic M, Sukhi A and Gurbel PA: Targeted pharmacotherapy for ischemia reperfusion injury in acute myocardial infarction. Expert Opin Pharmacother 21: 1851-1865, 2020.
4. Xiong YY, Gong ZT, Tang RJ and Yang YJ: The pivotal roles of exosomes derived from endogenous immune cells and exogenous stem cells in myocardial repair after acute myocardial infarction. Theranostics 11: 1046-1058, 2021.
5. Chen M, Li X, Yang H, Tang J and Zhou S: Hype or hope: Vagus nerve stimulation against acute myocardial ischemia-reperfusion injury. Trends Cardiovasc Med 30: 481-488, 2020.
6. Yellon DM and Hausenloy DJ: Myocardial reperfusion injury. N Engl J Med 357: 1121-1135, 2007.
7. Keeley EC, Boura JA and Grines CL: Primary angioplasty versus intravenous thrombolytic therapy for acute myocardial infarction: A quantitative review of 23 randomised trials. Lancet 361: 13-20, 2003.
8. Hausenloy DJ and Yellon DM: Myocardial ischemia-reperfusion injury: A neglected therapeutic target. J Clin Invest 123: 92-100, 2013.
9. Davidson SM, Ferdinandy P, Andreadou I, Bøtker HE, Heusch G, Ibáñez B, Ovize M, Schulz R, Yellon DM, Hausenloy DJ, *et al*: Multitarget strategies to reduce myocardial ischemia/reperfusion injury: JACC review topic of the week. J Am Coll Cardiol 73: 89-99, 2019.
10. Chang JC, Lien CF, Lee WS, Chang HR, Hsu YC, Luo YP, Jeng JR, Hsieh JC and Yang KT: Intermittent hypoxia prevents myocardial mitochondrial Ca^{2+} overload and cell death during ischemia/reperfusion: The role of reactive oxygen species. Cells 8: 564, 2019.
11. Kawaguchi M, Takahashi M, Hata T, Kashima Y, Usui F, Morimoto H, Izawa A, Takahashi Y, Masumoto J, Koyama J, *et al*: Inflammasome activation of cardiac fibroblasts is essential for myocardial ischemia/reperfusion injury. Circulation 123: 594-604, 2011.
12. Wallert M, Ziegler M, Wang X, Maluenda A, Xu X, Yap ML, Witt R, Giles C, Kluge S, Hortmann M, *et al*: α-Tocopherol preserves cardiac function by reducing oxidative stress and inflammation in ischemia/reperfusion injury. Redox Biol 26: 101292, 2019.
13. Sun X, Wei Z, Li Y, Wang J, Hu J, Yin Y, Xie J and Xu B: Renal denervation restrains the inflammatory response in myocardial ischemia-reperfusion injury. Basic Res Cardiol 115: 15, 2020.
14. Ong SB, Hernández-Reséndiz S, Crespo-Avilan GE, Mukhametshina RT, Kwek XY, Cabrera-Fuentes HA and Hausenloy DJ: Inflammation following acute myocardial infarction: Multiple players, dynamic roles, and novel therapeutic opportunities. Pharmacol Ther 186: 73-87, 2018.
15. Chen X, Li X, Zhang W, He J, Xu B, Lei B, Wang Z, Cates C, Rousselle T and Li J: Activation of AMPK inhibits inflammatory response during hypoxia and reoxygenation through modulating JNK-mediated NF-κB pathway. Metabolism 83: 256-270, 2018.
16. Chen J, Jiang Z, Zhou X, Sun X, Cao J, Liu Y and Wang X: Dexmedetomidine preconditioning protects cardiomyocytes against hypoxia/reoxygenation-induced necroptosis by inhibiting HMGB1-mediated inflammation. Cardiovasc Drugs Ther 33: 45-54, 2019.
17. Dong X, Fu J, Yin X, Cao S, Li X, Lin L, Huyiligeqi and Ni J: Emodin: A review of its pharmacology, toxicity and pharmacokinetics. Phytother Res 30: 1207-1218, 2016.
18. Dong X, Zeng Y, Liu Y, You L, Yin X, Fu J and Ni J: Aloe-emodin: A review of its pharmacology, toxicity, and pharmacokinetics. Phytother Res 34: 270-281, 2020.
19. Ye B, Chen X, Dai S, Han J, Liang X, Lin S, Cai X, Huang Z and Huang W: Emodin alleviates myocardial ischemia/reperfusion injury by inhibiting gasdermin D-mediated pyroptosis in cardiomyocytes. Drug Des Devel Ther 13: 975-990, 2019.
20. Li Q, Gao J, Pang X, Chen A and Wang Y: Molecular mechanisms of action of emodin: As an anti-cardiovascular disease drug. Front Pharmacol 11: 559607, 2020.
21. Bartel DP: MicroRNAs: Genomics, biogenesis, mechanism, and function. Cell 116: 281-297, 2004.
22. Hu F, Zhang S, Chen X, Fu X, Guo S, Jiang Z and Chen K: MiR-219a-2 relieves myocardial ischemia-reperfusion injury by reducing calcium overload and cell apoptosis through HIF1α/NMDAR pathway. Exp Cell Res 395: 112172, 2020.
23. Zhang C, Liang R, Gan X, Yang X, Chen L and Jian J: MicroRNA-384-5p/beclin-1 as potential indicators for epigallocatechin gallate against cardiomyocytes ischemia reperfusion injury by inhibiting autophagy via PI3K/Akt pathway. Drug Des Devel Ther 13: 3607-3623, 2019.
24. Chen Z, Su X, Shen Y, Jin Y, Luo T, Kim IM, Weintraub NL and Tang Y: MiR322 mediates cardioprotection against ischemia/reperfusion injury via FBXW7/notch pathway. J Mol Cell Cardiol 133: 67-74, 2019.
25. Yu SY, Dong B, Fang ZF, Hu XQ, Tang L and Zhou SH: Knockdown of lncRNA AK139328 alleviates myocardial ischaemia/reperfusion injury in diabetic mice via modulating miR-204-3p and inhibiting autophagy. J Cell Mol Med 22: 4886-4898, 2018.
26. Livak KJ and Schmittgen TD: Analysis of relative gene expression data using real-time quantitative PCR and the 2(-Delta Delta C(T)) method. Methods 25: 402-408, 2001.
27. Tong Z, Cui Q, Wang J and Zhou Y: TransmiR v2.0: An updated transcription factor-microRNA regulation database. Nucleic Acids Res 47 (D1): D253-D258, 2019.
28. Wang LJ, Qiu BQ, Yuan MM, Zou HX, Gong CW, Huang H, Lai SQ and Liu JC: Identification and validation of dilated cardiomyopathy-related genes via bioinformatics analysis. Int J Gen Med 15: 3663-3676, 2022.
29. Ogier-Denis E, Fasseu M, Vandewalle A and Laburthe M: MicroRNAs and intestinal pathophysiology. Med Sci (Paris) 23: 509-514, 2007.
30. Yu LM, Dong X, Xue XD, Xu S, Zhang X, Xu YL, Wang ZS, Wang Y, Gao H, Liang YX, *et al*: Melatonin attenuates diabetic cardiomyopathy and reduces myocardial vulnerability to ischemia-reperfusion injury by improving mitochondrial quality control: Role of SIRT6. J Pineal Res 70: e12698, 2021.
31. Ekshyyan O and Aw TY: Apoptosis in acute and chronic neurological disorders. Front Biosci 9: 1567-1576, 2004.
32. Atreya I, Atreya R and Neurath MF: NF-kappaB in inflammatory bowel disease. J Intern Med 263: 591-596, 2008.
33. Huang Q, Lu G, Shen HM, Chung MC and Ong CN: Anti-cancer properties of anthraquinones from rhubarb. Med Res Rev 27: 609-630, 2007.
34. Zhu T, Zhang W, Feng SJ and Yu HP: Emodin suppresses LPS-induced inflammation in RAW264.7 cells through a PPARγ-dependent pathway. Int Immunopharmacol 34: 16-24, 2016.
35. Zhu X, Zeng K, Qiu Y, Yan F and Lin C: Therapeutic effect of emodin on collagen-induced arthritis in mice. Inflammation 36: 1253-1259, 2013.
36. Ding QH, Ye CY, Chen EM, Zhang W and Wang XH: Emodin ameliorates cartilage degradation in osteoarthritis by inhibiting NF-κB and Wnt/β-catenin signaling in-vitro and in-vivo. Int Immunopharmacol 61: 222-230, 2018.
37. Chen GL, Zhang JJ, Kao X, Wei LW and Liu ZY: Emodin ameliorates lipopolysaccharides-induced corneal inflammation in rats. Int J Ophthalmol 8: 665-669, 2015.
38. Kitano A, Saika S, Yamanaka O, Ikeda K, Okada Y, Shirai K and Reinach PS: Emodin suppression of ocular surface inflammatory reaction. Invest Ophthalmol Vis Sci 48: 5013-5022, 2007.
39. Wu Y, Tu X, Lin G, Xia H, Huang H, Wan J, Cheng Z, Liu M, Chen G, Zhang H, *et al*: Emodin-mediated protection from acute myocardial infarction via inhibition of inflammation and apoptosis in local ischemic myocardium. Life Sci 81: 1332-1338, 2007.

40. McCarroll CS, He W, Foote K, Bradley A, McGlynn K, Vidler F, Nixon C, Nather K, Fattah C, Riddell A, *et al*: Runx1 deficiency protects against adverse cardiac remodeling after myocardial infarction. Circulation 137: 57-70, 2018.
41. Li X, Zhang S, Wa M, Liu Z and Hu S: MicroRNA-101 protects against cardiac remodeling following myocardial infarction via downregulation of runt-related transcription factor 1. J Am Heart Assoc 8: e013112, 2019.
42. Cui Y, Chen LJ, Huang T, Ying JQ and Li J: The pharmacology, toxicology and therapeutic potential of anthraquinone derivative emodin. Chin J Nat Med 18: 425-435, 2020.
43. Oshida K, Hirakata M, Maeda A, Miyoshi T and Miyamoto Y: Toxicological effect of emodin in mouse testicular gene expression profile. J Appl Toxicol 31: 790-800, 2011.
44. Ghafouri-Fard S, Shoorei H and Taheri M: Non-coding RNAs participate in the ischemia-reperfusion injury. Biomed Pharmacother 129: 110419, 2020.
45. Suzuki HI and Miyazono K: Emerging complexity of microRNA generation cascades. J Biochem 149: 15-25, 2011.
46. Fan ZX and Yang J: The role of microRNAs in regulating myocardial ischemia reperfusion injury. Saudi Med J 36: 787-793, 2015.
47. Ong SB, Katwadi K, Kwek XY, Ismail NI, Chinda K, Ong SG and Hausenloy DJ: Non-coding RNAs as therapeutic targets for preventing myocardial ischemia-reperfusion injury. Expert Opin Ther Targets 22: 247-261, 2018.
48. Xing X, Guo S, Zhang G, Liu Y, Bi S, Wang X and Lu Q: miR-26a-5p protects against myocardial ischemia/reperfusion injury by regulating the PTEN/PI3K/AKT signaling pathway. Braz J Med Biol Res 53: e9106, 2020.
49. Wang JX, Zhang XJ, Li Q, Wang K, Wang Y, Jiao JQ, Feng C, Teng S, Zhou LY, Gong Y, *et al*: MicroRNA-103/107 regulate programmed necrosis and myocardial ischemia/reperfusion injury through targeting FADD. Circ Res 117: 352-363, 2015.
50. Zhao J, Li X, Hu J, Chen F, Qiao S, Sun X, Gao L, Xie J and Xu B: Mesenchymal stromal cell-derived exosomes attenuate myocardial ischaemia-reperfusion injury through miR-182-regulated macrophage polarization. Cardiovasc Res 115: 1205-1216, 2019.
51. Hullinger TG, Montgomery RL, Seto AG, Dickinson BA, Semus HM, Lynch JM, Dalby CM, Robinson K, Stack C, Latimer PA, *et al*: Inhibition of miR-15 protects against cardiac ischemic injury. Circ Res 110: 71-81, 2012.
52. Chaudhuri AD, Choi DC, Kabaria S, Tran A and Junn E: MicroRNA-7 regulates the function of mitochondrial permeability transition pore by targeting VDAC1 expression. J Biol Chem 291: 6483-6493, 2016.
53. Shao W, Zhang SZ, Tang M, Zhang XH, Zhou Z, Yin YQ, Zhou QB, Huang YY, Liu YJ, Wawrousek E, *et al*: Suppression of neuroinflammation by astrocytic dopamine D2 receptors via αB-crystallin. Nature 494: 90-94, 2013.